

# Functional Cerebral Neurovascular Mapping During Focused Ultrasound Peripheral Neuromodulation of Neuropathic Pain

Stephen A. Lee<sup>ID</sup>, *Student Member, IEEE*, Hermes A. S. Kamimura<sup>ID</sup>, *Member, IEEE*, Mila Smith<sup>ID</sup>, and Elisa E. Konofagou<sup>ID</sup>, *Fellow, IEEE*

**Abstract**—**Background:** Nociceptive pain is required for healthy function, yet, neuropathic pain (disease or injury) can be severely debilitating. Though a wide-array of treatment options are available, they are often systemic and/or invasive. As a promising neuromodulation treatment, Focused ultrasound (FUS) is a noninvasive and highly spatially-targeted technique shown to stimulate neural activity, yet, effects on pain signaling are currently unknown. **Objective:** Develop and validate a method for studying FUS nerve stimulation modulation of pain-evoked neural responses *in vivo*. **Methods:** We developed a high-resolution functional ultrasound (fUS) method capable of mapping cortical responses in healthy and neuropathic pain mice in response to FUS neuromodulation treatment. **Results:** FUS-evoked hemodynamic responses are correlated with the intensity of peripheral neuromodulation. We confirm functional connectivity is altered in neuropathic mice and demonstrate that FUS can modulate neuropathic pain-evoked hemodynamics. **Conclusions:** The findings presented herein provides evidence for an FUS-based nerve pain method and validates the fUS technique developed for monitoring pain-evoked hemodynamics. **Significance:** We anticipate that the findings presented herein describe a noninvasive and flexible nerve modulation technique for pain mitigation, furthering evidence for clinical translation.

**Index Terms**—Functional ultrasound, focused ultrasound, peripheral nerve stimulation, neuropathic pain.

## I. INTRODUCTION

A S OUR primary sensory neurons are responsible for safely traversing our environment, the fundamental neurological

Manuscript received 2 September 2023; revised 21 November 2023; accepted 5 January 2024. Date of publication 10 January 2024; date of current version 13 May 2024. This work was supported in part by the National Institutes on Drug Abuse under Grant R36DA054475, in part by the National Institute of Biomedical Imaging and Bioengineering under Grant R01EB009041, in part by the Defense Advanced Research Projects Agency under Grant HR0011-15-2-0054, in part by the Focused Ultrasound Foundation, and in part by Google X, Inc. (*Corresponding author: Elisa E. Konofagou*.)

Stephen A. Lee, Hermes A. S. Kamimura, and Mila Smith are with Columbia University, USA.

Elisa E. Konofagou is with Columbia University, New York, NY 10032 USA (e-mail: ek2191@columbia.edu).

This article has supplementary downloadable material available at <https://doi.org/10.1109/TBME.2024.3352025>, provided by the authors.

Digital Object Identifier 10.1109/TBME.2024.3352025

understanding and recording of how we experience our sensations, especially pain, directly supplements the translation of these findings to the development of new neurological treatments. Yet, despite centuries of neuroimaging efforts and the development of several novel therapeutics, the understanding of the mechanisms involved in stimulated neural regulation is still in its infancy, especially for neuropathic pain signals. Meanwhile, an increased body of evidence points to neuromodulation as a key method for reversibly altering the activity of such afflicted neurons [1].

In neuropathic pain, dysfunction, whether by disease or injury, of the peripheral nervous system (PNS) can cascade into numerous functional changes in the brain, further contributing to acute and chronic pain. Among these changes, studies have observed spontaneous and ectopic action potentials which may trigger alterations in peripheral neurons and spinal cord circuits, where initial pain processing occurs [1]. Reversible neuromodulation can not only provide physical, but also both mental and economic relief as individuals with neuropathic pain often develop secondary ailments, such as depression, requiring constant medication and hospital visits [1].

FUS offers a noninvasive alternative to electrical or infrared stimulation, seeing rapid progress as an interventional neuromodulation modality [2]. The popularity of this technique is reflected in its wide-spread investigation, with several studies highlighting changes in neural potentiation [2], [3], [4], [5], [6], [7], [8], [9], [10] in various animal models [7], [11], [12], [13], [14], [15], [16], [17], [18]. While these observations are indeed promising, direct clinical implications towards neuropathic pain are still limited. Thus, key questions remain, barring clinical translation – namely, (1) does FUS nerve stimulation operate similarly to other somatosensory stimuli and (2) can FUS modulate pain activity in neuropathic pain models?

Functional ultrasound (fUS) can map somatosensory activation with high temporal resolution and unparalleled access to whole-brain images at depth. Similar to fMRI, fUS utilizes the changes in cerebral blood volume (CBV) via neurovascular coupling as a correlate of neural activity [19], [20]. In contrast to optical methods, fUS can image across the entire brain and, counter to fMRI, can operate in real-time, measuring more transient and/or rapid signals with high temporal and spatial resolution [21]. Currently, however, fUS may still lack the

appropriate sensitivity when it comes to measuring and quantifying pain signaling from the periphery to the cortex. Evidence suggests that neurovascular coupling is highly linked to changes in capillaries, the smallest vessels in the microvasculature [22], [23]. Thus, to ensure success in imaging activity to FUS nerve stimulation, where the projections and representation in the brain is unknown, a fUS methodology with higher sensitivity to small blood vessels, such as increasing the center frequency, is warranted.

Here, we address this limitation through the development of a high-resolution fUS method to elucidate the dynamics of neuropathic pain-evoked neural hemodynamics via FUS nerve stimulation. By applying continuous, real-time monitoring of CBV, we first demonstrate that FUS peripheral neuromodulation, similar to electrical stimulation, is capable of evoking cerebral activity, demonstrating that greater CBV changes are correlated with larger muscle activation. Lastly, we investigated fUS-associated changes in spared nerve injury (SNI) mice models of acute neuropathic pain with and without FUS nerve modulation. We elucidate changes through combinations of sham-surgery and sham-FUS in SNI and wild-type mice, highlighting notable changes in cortical activity.

## II. METHODS & MATERIALS

### A. Animals

All experiments were performed in accordance with the Columbia University Institutional Animal Care and Use Committee (Protocol # AAA-Z0451; approval 2023-02-01). Female C57BL/6 J mice (Envigo; Indianapolis, IN, USA) ages 8 – 10 weeks were used in all experiments and kept to the absolute minimum. For experiments with wild-type mice: n = 10 total (n = 2 whisker stimulation, n = 3 electric paw stimulation, n = 3 FUS stimulation, n = 2 FUS + electrical stimulation). For experiments with SNI neuropathic pain model mice: n = 9 total (n = 3 sham surgery, n = 3 SNI positive controls, n = 3 SNI experimental). Mice were housed in rooms with 12 h light/dark cycles and provided food and water ad-lib.

Animals were anesthetized using isoflurane (2% for induction; 0.8 – 1% for experimentation; 0.8% flowrate). Body temperature was kept at 37 °C, respiratory rate was monitored, and isoflurane % was modulated to achieve continuous breathing without gasping. This method allowed for mitigation, and in most cases, elimination of breathing artifacts within fUS imaging. A large-window craniotomy was performed to expose the whole brain.

### B. Spared Nerve Injury

Animals underwent sterile surgical manipulation at least 10 days before imaging to allow for adequate development of neuropathic pain. Briefly, animals were anesthetized with 2% isoflurane and positioned prone with the spine facing upwards. Before opening the skin, 2 mg/kg Bupivacaine was subcutaneously injected into the area. Afterwards, an incision was made and blunt dissection was used to expose the sciatic trifurcation. Here silk 6–0 suture was used to ligate the common peroneal

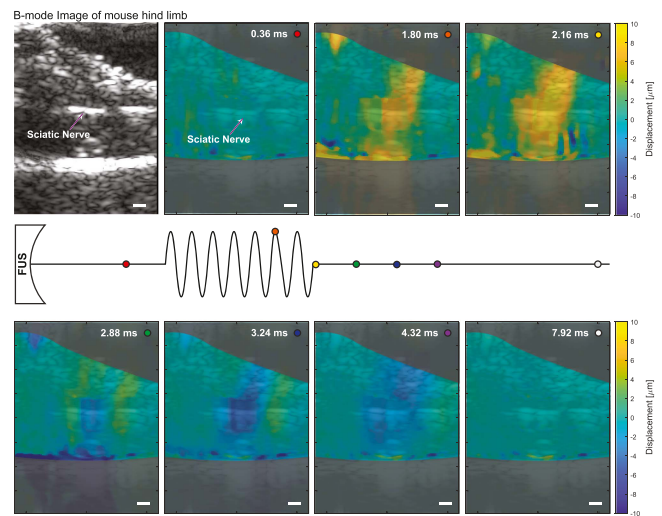


**Fig. 1.** Displacement imaging overlaid onto B-mode images for targeting of the sciatic nerve via confocal FUS and imaging system. Different time-points along the FUS stimulation waveform are shown in the still frames. Downward displacement is seen as positive displacement (away from the transducer). Scale bar = 1 mm.

and tibial trunks and a 2 mm section was dissected out to prevent nerve regrowth. Animals were sutured up and monitored continuously until awake. Animals were checked every 24 h for any behavioral anomalies and suture removals [24].

Mice were tested via von-Frey sensory testing before (day 0) and after (days 2 – 14) SNI surgery until functional imaging sessions. They were allowed to acclimate to the room for at least 30 minutes before von-Frey testing on a wire-mesh platform. Fibers of increasing deflection forces starting at 0.04 g were used to mechanically stimulate the mouse hind paw in both legs. Withdrawal or pain-indicating behaviors, like paw-licking, were counted as a pain response. The 5 stimulations were applied within 2 minutes and separated by at least 10 seconds. Withdrawal ratios were taken as a ratio between the threshold of the right, ipsilateral to the surgery, to the threshold of the left, contralateral. The whole time course of the experiments can be seen in Fig. 2.

### C. Stimulation Paradigms

After the craniotomy, somatosensory stimulation was set up immediately Fig. 2(a). Whisker stimulation was performed using a 5 s, 10 Hz, 50% duty cycle stimulation waveform to actuate the vibrissae. In a separate experiment, electric hind limb stimulation was performed using a bipolar needle electrode (EL415; Biopac, Goleta, CA, USA) driven by an isolated pulse stimulator (Model 2100; A-M Systems, Sequim, WA, USA). The needle was implanted into the dermis of the glabrous skin in the hind paw, and a 2 mA, 5 ms bipolar electrical pulse at 5 Hz for 5 seconds was delivered. For the neuropathic pain paired pulse stimulation experiment (Fig. 2(b)), up to 2 mA, 10 Hz, 10 seconds, 10% DC electrical pulses were used for each pulse train. Stimulation amplitude was increased until a visible muscle activation was seen.

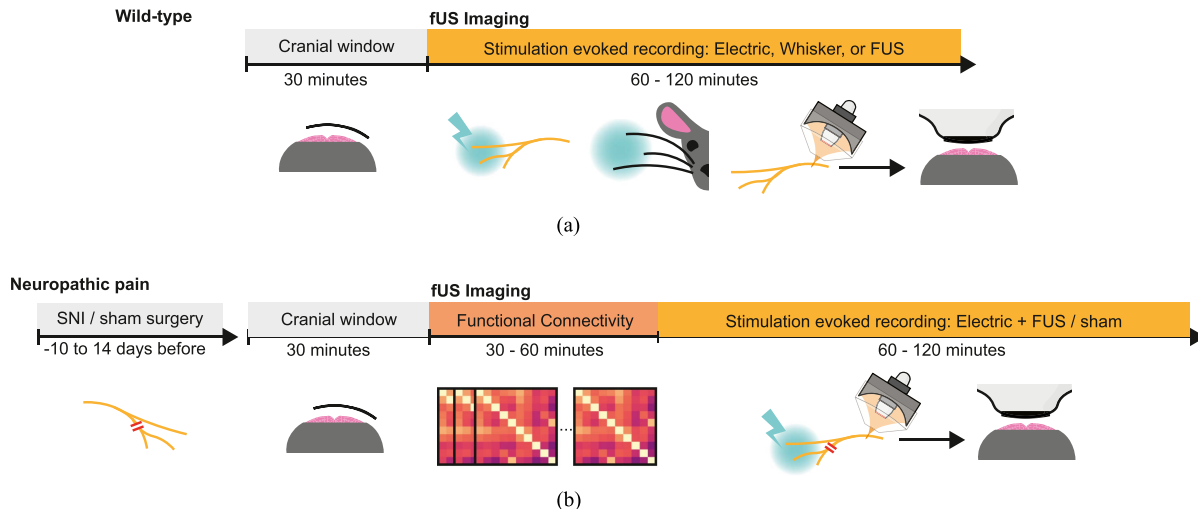


**Fig. 2.** Timeline of stimulation and fUS recording experiments. **(a)** Experimental time course for electrical, whisker, or focused ultrasound stimulation of wild-type mice. **(b)** Time course for experiments involving neuropathic pain spared-nerve injury models. SNI surgery takes place at least 10 days before fUS recording. Before electrical stimulation of the hind paw and FUS stimulation of the sciatic nerve, resting-state fUS recordings were taken for post-hoc functional connectivity analysis.

FUS was performed using a 3.1 MHz focused transducer. A focusing cone with an acoustic-permeable membrane was filled with degassed water to couple the transducer face with the skin of the hind limb. The transducer was driven by a function generator (33220a, Agilent, Santa Clara, CA, USA) and an RF amplifier (A150, E&I, Rochester, NY, USA) combination. To elicit a compound muscle activation, one single 1 ms, 9.57 MPa derated rarefactional pressure FUS pulse was delivered to the sciatic nerve non-invasively. The FUS focal size is 3 mm x 0.6 mm full-width half-max (FWHM). The hind limbs were first shaved, and depilatory cream was used to remove all hair from the delivery site. B-mode imaging and displacement targeting [7], [25] was used to identify the sciatic nerve and confirm delivery of the ultrasound (Fig. 1). Once positioning was sufficient to elicit robust and continuous neuromodulation, a train of 5 pulses using the previously defined parameters at 1 Hz was used during the fUS imaging experiments (Supplemental Video S4). For neuropathic pain mice, PRF was increased to 10 Hz and the sonication duration to 10 s (0.1% DC effective). The maximum  $I_{SPTA}$ ,  $I_{SPPA}$ , and mechanical index used in the study were 3.2 mW/cm<sup>2</sup>, 3.2 W/cm<sup>2</sup>, and 5.65, respectively.

#### D. Ultrasonic Imaging of the Mouse Brain

After the somatosensory stimulus was set up, the gauze covering was removed, and degassed ultrasound gel was placed on the brain. The 256-element, 40 MHz linear transducer (MS550D, FujiFilm VisualSonics, Toronto, Ontario, Canada) was placed on the brain. The transducer was connected to an ultrasound scanner (Vantage-256 High-Frequency Option, Verasonics, Kirkland, WA, USA) and Matlab (Mathworks, Natick, Massachusetts, USA) was used to program custom transmit and receive acquisitions. The transducer elevational width and natural focal depth of this transducer were 0.458 mm and 5 mm, respectively. The real-time operation was enabled using a GPU (P6000; Nvidia, Santa Clara, CA, USA) and the CUDA API. At the beginning of

each session, an anteroposterior 1D raster scan is performed to find the desired cortical structure by visually matching cortical and subcortical vessel organization. In this study, functional imaging was performed at Bregma -0.5, -1.2, and -1.5 mm (negative indicates caudal).

During the course of this study, functional ultrasound was performed using two acquisition schemes: event-locked (whisker and electrical) or continuous acquisition (FUS). A single Doppler image was acquired for event-locking sequences at a specific time relative to a single somatosensory stimuli event timed using a microcontroller. Tracking functional CBV changes using this method allowed for 10 Hz sampling, but it is time-consuming if acquiring at high temporal resolutions and long stimuli sequence times ( $\leq 1$  h for a single stimulus). Continuous acquisition was performed through GPU-accelerated Stolt-FK migration beamforming [26] in lieu of conventional delay-and-sum beamforming. RF data was acquired at 3/4th the sampling frequency to alias the high-frequency signal and then spectrum flipped around the center frequency [27]. Briefly, RF data at the now 1/4th sampling frequency was Fourier transformed into frequency/k-space and migrated using delays dictated by the exploding reflector model (ERM), interpolated, and then transformed back. Speedup over CPU processing was achieved using Matlab's mex formats and CUDA's cuFFT library. Coherent compounding of ultrasound images was also completed using a separate kernel on the GPU. A speedup of 100% was achieved compared to GPU DAS (benchmarked using a Tesla K40c GPU). Further speedup can be achieved through the use of overlapping kernelsstreams or multi-GPU functionality. Migration of DAS to FK-migration enabled a 1 Hz display rate after beamforming, processing data from all 256-elements, and saving the CBV image.

Ultrasound imaging sequences consist of 7 tilted (4 cycles) plane wave transmits evenly spaced between  $\pm 7^\circ$  (continuous) or  $\pm 14^\circ$  (event-locked). Plane waves were sent at a 500 Hz compounded PRF: 3500 Hz at  $7^\circ$  or 7000 Hz at  $14^\circ$ . Each received

RF stack consisted of 200 compound frames (event-locked) or 120 compounded frames (continuous). The maximum  $I_{SPTA}$  and  $I_{SPPA}$  of the fUS parameters explored in this study were 19.15 mW/cm<sup>2</sup> and 9.12 mW/cm<sup>2</sup>, respectively and the MI was 0.08 which all are below the FDA limit for ultrasonic imaging. The number of time samples was set to reconstruct at least 4 mm of the mouse brain. However, to achieve even faster processing time, the field of view can be limited to just the cortex, decreasing the number of samples and the size of the reconstruction grid. After acquiring and beamforming compounded RF stacks, a spatiotemporal filter using the singular value decomposition [21] was used to remove tissue signals and reconstruct only the blood signals. Since breathing movement artifacts rarely introduced noise into the images, eigenvalues below 50 were removed in both schemes to balance signal power and removal of tissue signal. Lastly, the reconstructed stack of beamformed RF was summed to illustrate the final CBV image.

### E. Functional Image Processing

Vessel resolution analysis was completed using python 3.7 and the Python Imaging Library (PIL) package. The intensity profile of a selected line across vessels was used to generate a Gaussian fit of individual vessels. The full-width half-max of the Gaussian distribution was used to estimate the vessel diameters. This process was repeated 5 times in each case to generate error and standard deviation of measurements. 3D renderings of vessel organization were constructed using open-source Paraview (Kitware, Clifton Park, New York, USA). 3D scans were acquired by 1D raster scanning in 0.1 mm steps.

Sequences of power Doppler, or CBV, images were acquired: 10 – 15 frames for baseline, 5 – 20 frames during the stimuli (dependent on fUS PRF and stimulus duration), and 10 – 15 frames for after. All stacks of CBV images were first low pass filtered (2nd order Butterworth) and  $\Delta$ CBV/CBV was calculated. Correlation maps of activation were constructed pixel-by-pixel using Pearson's correlation coefficient  $r$  between the power Doppler signal and the binary stimuli signal. Correlation values above  $r > 0.193$  were chosen as statistically significant activation pixels. Final correlation maps were acquired after median filtering. Lastly, stereotaxic brain maps (Allen Brain Atlas; Allen Institute, Seattle, WA, USA) were overlaid onto functional ultrasound images so that ROI can be selected from the targeted brain regions. The average CBV traces of the region were then measured to determine the magnitude of somatosensory stimulation. Using these CBV curves, AUC analysis was performed by integrating the increase of CBV after sensory stimulation has initiated. For analysis of CBV changes in cortical layers, CBV changes that reach higher than 1 STD of the baseline signal underwent AUC analysis.

### F. Neuropathic Pain Analysis

Functional connectivity maps were constructed by recording 30–60 minutes of resting-state hemodynamics (Fig. 2(b)) at 2 Hz functional frame-rate [28]. Regions of the S1HL, M1, M2, Cg1, and Cg2 for the left and right hemispheres were manually segmented. Individual functional connectivity maps

were constructed by correlating the average temporal signal at each region with each other. Corresponding maps for SNI-sham and neuropathic pain mice were averaged together to show overall differences between the two groups.

Videos of paw twitches were recorded using a 1080p webcam at 30 frames per second (C920; Logitech, Lausanne, Switzerland). The Vantage Matlab software triggered video recording at the beginning of the paw twitches. Matlab's Computer Vision Package was used to generate difference maps and motion vectors of paw movement. Motion vectors are given in pixels/frames and were converted to pixels/s. The average motion vector value of all paw twitches in a single train of FUS stimulation was used for correlation analysis.

### G. Statistical Testing

All statistical analysis was conducted using GraphPad Prism 9.3. For the correlation between paw movement and CBV, a nonparametric Spearman correlation (two-tailed, 95% confidence interval) was used to establish the relationship between hind-limb cortex AUC and paw velocity. All analysis in neuropathic pain mice were completed using a two-way ANOVA with multiple comparisons and Holm-Sidak correction. Summary data is presented as a  $\Delta$ CBV from pre-FUS measurements. Statistics on functional connectivity was conducted on average correlations maps for SNI-sham and neuropathic pain groups (SNI-FUS, FUS-sham). Again, a two-way ANOVA with multiple comparisons and Holm-Sidak correction was used.

## III. RESULTS

The high-resolution technique was designed for straightforward experimental implementation and stable hemodynamic recording through a large cranial window in wild-type (C57BL/6 J) mice (Fig. 3(a)). A 256-element linear array transducer with a 20 mm footprint, operating at a 40 MHz center frequency, acquired stacks of beamformed anatomical ultrasound images at 3500 Hz and filtered using a spatiotemporal singular value decomposition (SVD) filter to remove stationary tissue signals. The remaining blood signals were integrated to generate a single CBV image (Fig. 3(b)). Sequences of CBV images were then acquired before, during, and after corresponding somatosensory stimulations to generate temporal hemodynamic traces. Once stimuli trials concluded, time-series hemodynamics were analyzed to visualize cortical activity patterns (CBV changes) evoked from mechanical, electrical, and FUS stimulations.

Before functional neuroimaging, brain recording sites were selected after one-dimensional raster scans throughout the cranial window for slice selection. In Fig. 3(c), vessels above 70  $\mu$ m in diameter in cortical and deeper subcortical regions were resolved without contrast agents. We see that vessels, tens of microns apart, within the focal volume can be distinguished, enabling the assessment of cortical health after craniotomy. 3D rendering further reveals how small and large vessels are organized, allowing for fine adjustment of the imaging plane to target the selected brain region for fUS imaging (Fig. 3(d); Supplemental Video S1).

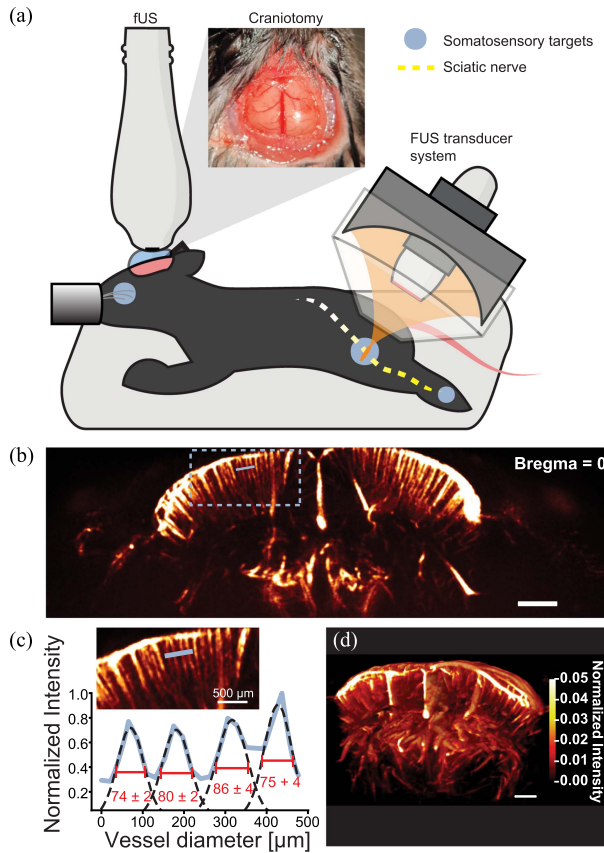


**Fig. 3.** High-resolution fUS imaging of FUS nerve stimulation. **(a)** Experimental diagram depicting transducer placement, large-window craniotomy, and whisker, electrical, or FUS stimulation targets. **(b)** Representative CBV image of vascular signals after spatiotemporal filtered tissue signal removal at Bregma = 0. Scale bar = 1 mm. **(c)** Vessel profiles and diameter analysis of intensity profile in microns. **(d)** 3D rendering of brain vasculature generated by 1D rostral/caudal scan at 0.1 mm scan resolution.

Neuroimaging of the response to FUS stimulation critically depends on the ability to confidently image established constructs and pathways, such as the whisker to barrel field (S1BF) or hind paw to hind limb (S1HL) cortex. Taking advantage of the higher resolution afforded by imaging at 40 MHz permits clearly articulated anatomical information in the small mouse brain [29], [30]. This translates directly to increased detection and localization of functional hemodynamic changes to somatosensory stimuli (Fig. 4(a); Supplemental Videos S2 and S3). Stimulation of the left whiskers resulted in a 40% peak increase in the contralateral S1BF cortex compared to baseline. Through pixel-based correlation between the whisker stimulation signal and hemodynamic traces, active regions (Fig. 4(b), left) and average contralateral and ipsilateral S1BF increases (Fig. 4(b), right) are identified. Likewise, Fig. 4(c) shows the corresponding correlation map under electric stimulation of the right hind-paw and hemodynamic patterns for the contralateral and ipsilateral S1HL cortex. Here, the electrical stimulation parameters used to evoke cortical responses generated a significant 60% peak increase in CBV in the contralateral hind-limb cortex. Additional correlated response patterns were also recorded in the adjacent fore-limb region and motor cortex.

### A. FUS Nerve Stimulation Evokes Cerebral Hemodynamic Responses

As stated before, a major obstacle in translating ultrasound for neuropathic pain treatment is the lack of evidence for cortical modulation as a result of the FUS application to the peripheral nerves. To verify this, we recorded hemodynamic activation patterns associated with FUS-mediated nerve neuromodulation (Fig. 5(a) and (b)). Here, successful neuromodulation was represented by measured displacement [7] and paw motor dorsiflexion (Fig. 5(b)). With each muscle contraction, fUS imaging showed that CBV in the contralateral S1HL did indeed increase (Fig. 5(c); Supplemental Video S4). Area-under-the-curve (AUC) analysis showed CBV changes of 9.46% in comparison with 1.02% in the contralateral and ipsilateral S1HL, respectively. This separation is mostly prominent during FUS application where contralateral hemodynamics increase more rapidly than in the ipsilateral hemisphere. While FUS stimulation evoked similar hemodynamic responses to electrical paw and whisker stimulation, it had significantly lower peak CBV (2% compared to 40–60%). This may be largely due to the fUS sensitivity of the scale difference in the stimulus duty cycle of the FUS (0.1% DC) compared to whisker (50% DC) and electrical (2.5% DC).

The experimental findings reported herein also highlight variance within sequential FUS pulses, where some sonifications failed to elicit a motor response. We were capable of successfully activating the sciatic nerve and subsequent paw stimulation in 100% of the sonicated mice. However, within each mouse, the success rate of activation for a train of 5 subsequent FUS pulses ranged from 20–100% dependent potentially on the anesthesia levels and baseline nerve activity. Therefore, we asked whether the intensity of the overall FUS stimulation was an indicator to the scale of hemodynamic responses observed. To objectively measure motor responses to FUS stimulation without interfering with the paw movement itself or introducing additional skin or muscle sensations – i.e., puncture of the skin via EMG electrodes – we performed video recording and analysis of the FUS-induced paw motion via vector motion analysis (Fig. 5(b)). Fig. 5(d) shows accordingly, larger paw twitches had greater associated CBV AUC measurements ( $p = 0.0215$ , two-tailed Spearman correlation). In addition, organizing the CBV changes into functional layers of the hind-limb cortex (Fig. 5(e)) showed that each layer's contribution. What Fig. 5(f) shows is that layers 4 and 5, the initial targets of sensory inputs and the first level of cortical processing, have greater CBV rates than other layers of  $1.34\% \pm 9.89\%$  and  $1.77\% \pm 11.18\%$  higher than one standard deviation of the baseline recordings, respectively.

### B. FUS Modulates Pain Signaling in Neuropathic Pain Mice

We next investigated the effects of FUS nerve stimulation in spared nerve injury models of neuropathic pain. Mice were separated into three groups of  $n = 3$  mice subjected 5 experimental trials each (SNI-sham [ $SNI^-/FUS^+$ ]; FUS-sham [ $SNI^+/FUS^-$ ]; and SNI-FUS [ $SNI^+/FUS^+$ ]). We performed surgical ligation and sectioning of the common peroneal

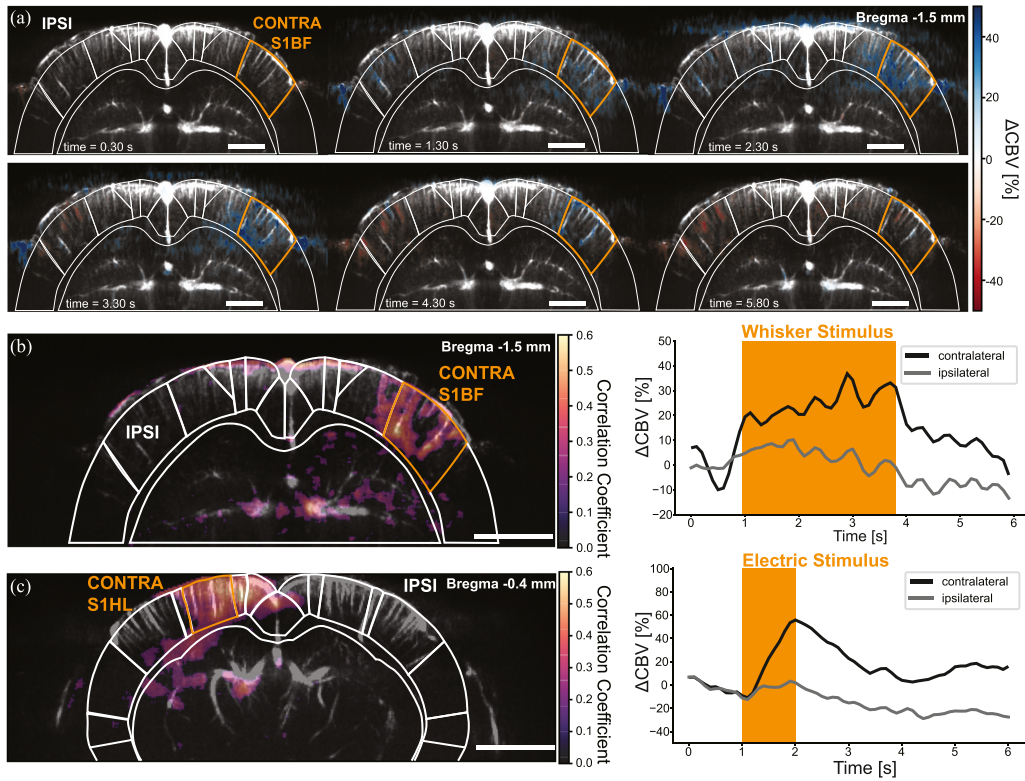


**Fig. 4.** fUS imaging can measure evoked responses from somatosensory stimulation. **(a)** Sequential images showing rise and fall of CBV in the barrel field cortex over time at Bregma  $-1.5\text{ mm}$ . Scale bar = 1 mm. **(b)** Left - Correlation maps generated from whisker (top) and electric hind limb (bottom) stimulation (Bregma  $-0.5\text{ mm}$ ). Average CBV measurements from the highlighted ROI and stimulus durations are shown on the right.

and tibial nerves, leaving the sural nerve intact. Afterwards, robust neuropathic pain in the regions innervated by the sural nerve (Fig. 6(a)) developed within 3 to 7 days. von-Frey sensory threshold testing at the sural receptive field was conducted to confirm neuropathic pain development. FUS-sham and SNI-FUS mice had increased levels of withdrawal in the ipsilateral paw compared to the contralateral (Fig. 6(b)). SNI control mouse 3 exhibited insensitivity to sural receptive field stimulation and thus was excluded from subsequent analysis. SNI-sham mice withdrawal ratios remained around 1.0, indicating no differential withdrawal thresholds in either paw [31]. After 10 days, the SNI sham and SNI control groups were imaged with fUS and the SNI FUS group was imaged 4 days later.

Functional connectivity between SNI-sham and neuropathic mice was conducted using the regions indicated in Fig. 6(c) by recording 30 minutes to an hour of resting state before experimentation. Fig. 6(d) shows that at the time of imaging, neuropathic pain mice had an overall decorrelation across the whole brain. Both left and right hemispheres had significantly lower correlations than in SNI-sham mice (Fig. 6(e)). If we examine each individual hemisphere, we see that the S1HL, M1, M2, and Cg2 regions in the left hemisphere and only the S1HL in the right hemisphere were significantly less correlated. These observations may be due to performing SNI surgery in the right hind limb.

To assess the potential of FUS neuromodulation in the treatment of neuropathic pain, a paired electrical pulse train stimulation scheme was used to electrically excite the hind paw at the

sural innervated receptive fields (Fig. 6(a)). Here, electric stimulation parameters ( $<2\text{ mA}$ , 10 Hz, 10 seconds, 10% DC) used to preferentially stimulate A fibers – not normally associated with activation of c fiber neurons in healthy animals – were selected to activate nociceptors in neuropathic pain mice [32]. FUS sonication parameters (9.57 MPa (derated), 10 Hz, 10 seconds, 1% DC) were increased from a previous experiment (see Supplementary Materials) to reflect current pulse sequences used in human peripheral neuromodulation [25]. This experiment was divided into three segments: before, during, and after FUS (Fig. 7(a)) and CBV recordings of the S1HL were sampled from the ROI depicted in Fig. 6(c) for each condition. Fig. 7(a) shows average responses for all mice over all three time points. Before FUS (pre-FUS), electrical stimulation increased CBV responses. In contrast to sham, neuropathic pain mice ( $SNI^+/FUS^-$ ,  $SNI^+/FUS^+$ ) had persistent elevated increases in S1HL CBV after the electrical stimulation. Only in sham mice did responses return to baseline.

During FUS/Sham sonication (Fig. 7(a) middle), sham mice experienced enhanced levels of hemodynamic flux. In the positive control group ( $SNI^+/FUS^-$ ), mice experienced no change in elevated levels from before FUS stimulation. However,  $SNI^+/FUS^+$  mice showed that FUS stabilized CBV throughout the electric stimulation (no further increases were observed after the 2nd electrical pulse train). At timepoint 3, post-FUS  $SNI^+/FUS^+$  CBV traces were similar to  $SNI^-$  sham mice. Moreover, average CBV traces for  $SNI^+/FUS^+$  mice, post-FUS were lower than their measurement pre-FUS,

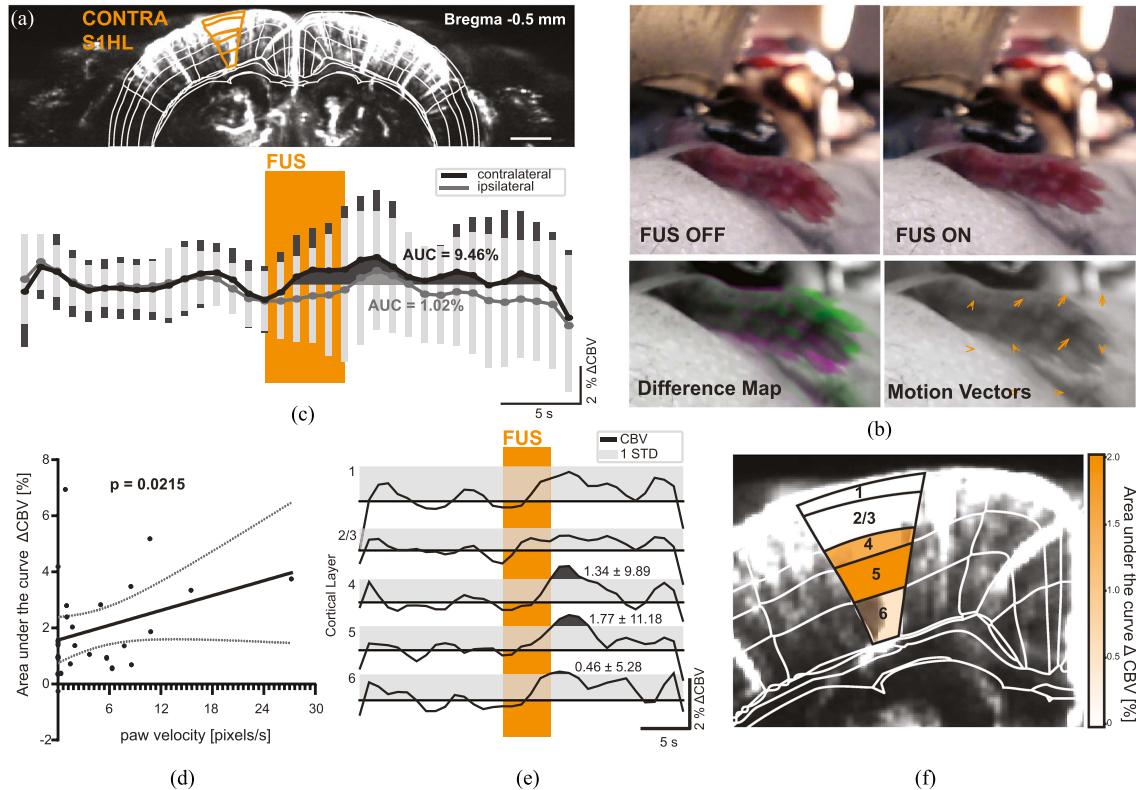


**Fig. 5.** FUS sciatic nerve neuromodulation induces hemodynamic changes and paw dorsiflexion. (a) Power Doppler vasculature image of the brain and overlaid stereotaxic functional map of Bregma  $-0.5$  mm (scale bar = 1 mm). (b) Two representative frames of FUS sciatic nerve neuromodulation before (left) and during FUS delivery (right). Paw movement analysis displayed as difference maps (left) and pixel vector motions (right). (c) CBV pattern in the contralateral and ipsilateral hind limb cortex evoked from FUS sciatic nerve stimulation ( $n = 3$  mice). (d) Correlation between CBV AUC and FUS-induced paw movement intensity using data from C and D (two-tailed non-parametric Spearman correlation;  $p = 0.0215$ ). (e) and (f) CBV increases from FUS stimulation organized by specific cortical layers (1, 2/3, 4, 5, and 6).

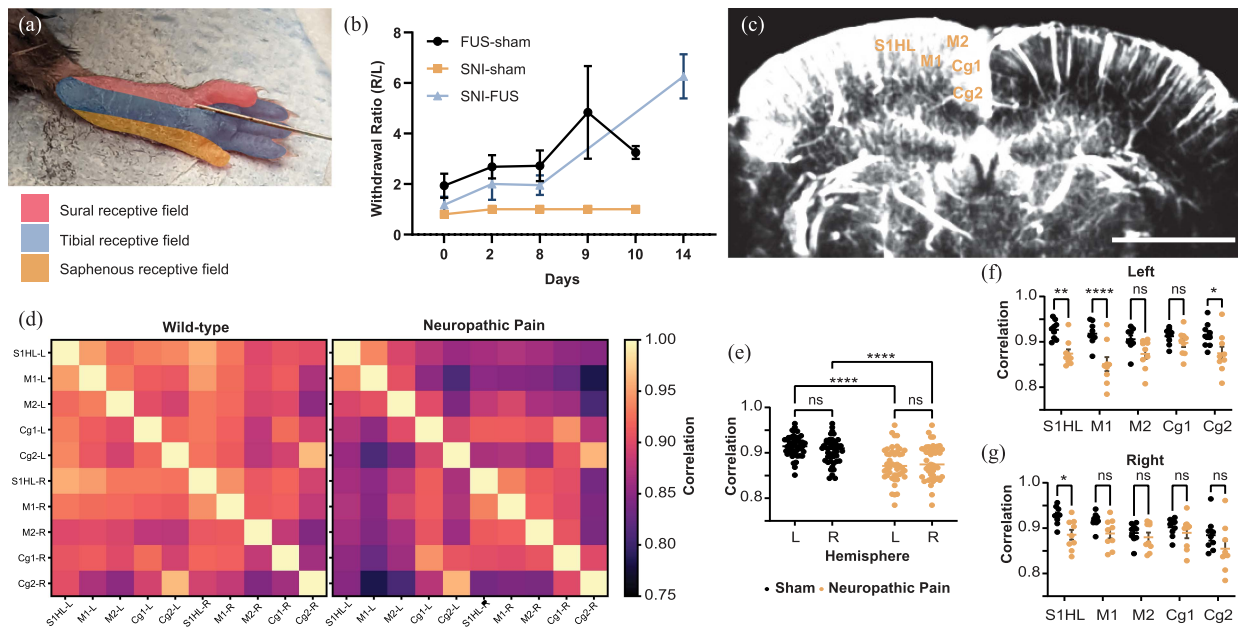


**Fig. 6.** Cerebral functional connectivity undergoes changes in SNI mice. (a) Receptive field of the sciatic nerve branches. (b) Von-frey sensory testing displayed as a ratio of withdrawal between right (ipsilateral) and left (contralateral) legs. (c) fUS map and corresponding brain regions for functional connectivity analysis (scale bar = 1 mm). (d) Average functional connectivity maps for wild-type mice (left) vs neuropathic pain mice (right). (e) Connectivity correlation differences between left and right hemispheres. (f) Correlation values for left hemisphere as indicated in (c). (g) Correlation values for right hemisphere regions opposite (f). In E-G, \* $p < 0.05$ , \*\* $p < 0.01$ , \*\*\* $p < 0.005$ , \*\*\*\* $p < 0.0001$  two-way ANOVA with multiple comparisons and Holm-Sidak correction for multiple comparisons.

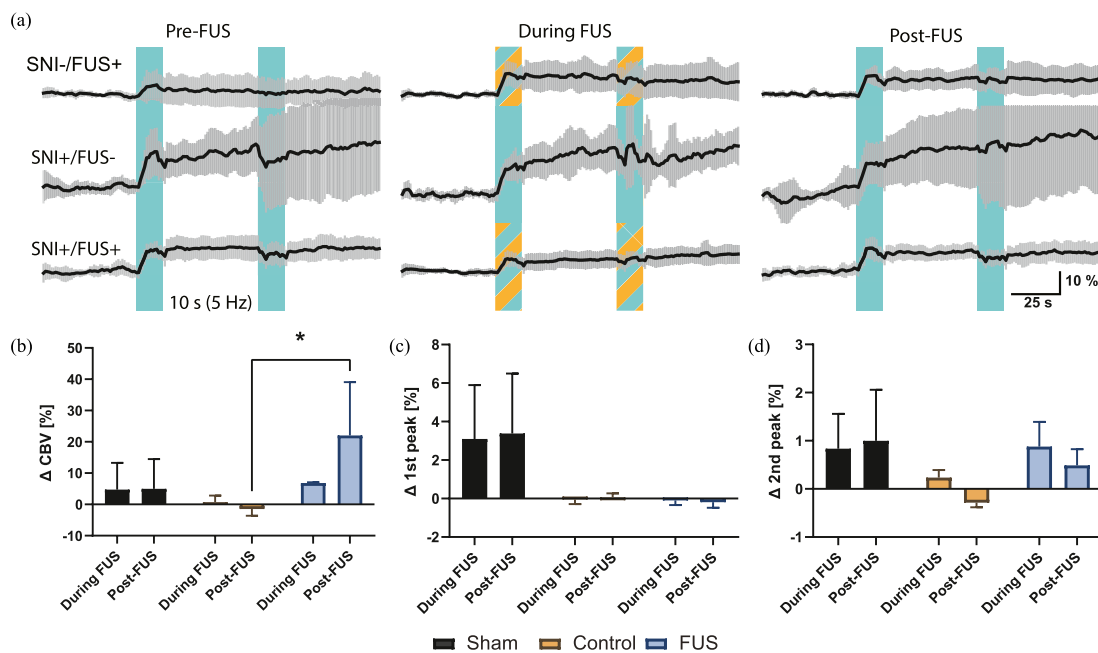


**Fig. 7.** FUS nerve neuromodulation of neuropathic pain in SNI model mice. (a) All CBV traces for all three groups (Top: SNI-sham; Middle: FUS-sham; Bottom: SNI-FUS) over three time-points (before, during, and after FUS) using paired pulse stimulation schemes. Striped vertical bars indicate simultaneous electrical and FUS application. (b) Comparison of resultant increase in cortical S1HL CBV after stimulations compared to baselines. (c) Cortical S1HL peak-to-peak comparisons for the first stimulation pulse. (d) peak-to-peak analysis for stimulation pulse 2. In B-D, \* $p < 0.05$  two-way ANOVA with multiple comparisons and Holm-Sidak correction for multiple comparisons.

demonstrating a stabilization of CBV changes that reflect behaviors in sham mice.

To quantify CBV behavioral changes, we present measurements of the overall  $\Delta\text{CBV}$ ,  $\Delta\text{peak 1}$ , and  $\Delta\text{peak 2}$  as a difference from baseline measurements (time point 1, pre-FUS). Fig. 7(b) shows that overall CBV in sham  $SNI^-/FUS^+$  mice were elevated at time points 2 and 3. In positive control  $SNI^+/FUS^-$  mice, there was a 6% increase during FUS but a 20% greater increases post-FUS, indicating that successive electrical stimulations may increase in pain over time. In contrast,  $SNI^+/FUS^+$  mice had almost no changes during and after FUS stimulation. In fact, there is a decrease in  $\Delta\text{CBV}$  at timepoint 3 between positive controls and the experimental group.

Since we were testing hemodynamic responses to conditional pain sensitivity over two pulses (similar to long term potentiation experiments), we analyzed the peak-to-peak differences during both electrical pulse trains. Unexpectedly, if we look during the first and second pulses we see moderate differences between SNI-sham and neuropathic pain groups (Fig. 7(c) and (d)). We found that sham mice experienced peak changes in both pulses, the first experiencing larger changes than the second. In contrast, SNI mice did not experience any changes in the first peak, i.e., the peak values stayed the same compared to baseline measurements. The differences lie in the second peak demonstrating that positive control mice had increased  $\Delta\text{peak}$  values than SNI mice that received FUS sciatic stimulation. In fact, the peak value decreased compared to baseline measurements after FUS was applied. These findings did not achieve statistical significance, however two-way ANOVA testing for subject variance was significant for both peak measurements

(1st peak:  $p < 0.0001$ , 2nd peak:  $p < 0.0165$ ), indicating that results may be under powered.

#### IV. DISCUSSION

The control of neural pain through noninvasive manipulation of nerve function without the use of injecting current or surgical intervention has major implications for how we provide personalized pain care as the average global age keeps rising. To shed light on possible mechanisms for FUS pain intervention, several novel developments had to be implemented. In this study, we developed a high-resolution ultrasound neuroimaging method to understand the effects of FUS nerve stimulation of cortical activity. The fUS approach offers a useful whole-brain, real-time, small animal neuroimaging approach with high spatial and temporal resolution and without the use of administered contrast agents. Although typical fUS studies operate at 15 MHz, giving spatial resolutions of 100  $\mu\text{m}$  [21], imaging at 40 MHz allows spatial resolution as low as 38.5  $\mu\text{m}$  [29], [30]. This allowed for recovering slightly smaller diameters (75 to 86  $\mu\text{m}$ ) and more cortical vessels per square millimeter. Indeed, with the increased fUS sensitivity our approach afforded, we saw that FUS sciatic nerve stimulation activates the S1HL region with lower activation than electric stimulation – indicating that FUS has a higher threshold of activation [33]. The mechanical force required to induce electrical changes may not be as consistent as current injection. The area of the observed response, nonetheless, is consistent with somatosensory-evoked potentials from the hind limb [34], [35]. We ascertain that FUS does have the capability of stimulating the corresponding brain circuits in the somatosensory hind limb cortex.

By stimulating the sciatic nerve, a mixed nerve bundle composed of sensory and motor fibers, FUS may be nonselective in exciting all fiber types. In fact, recent ex vivo analysis of FUS nerve stimulation confirms mechanical activation of a variety of fibers involved in touch [33]. Interestingly, our data indicates that in the absence of other stimuli, FUS can excite functional activity. As previous studies have shown, factors such as the underlying biology (ion channel distribution, fiber type) or the FUS parameters (carrier frequency, intensity, pulse duration, pulse repetition frequency) used for modulation may be the underlying culprit for the wide range, and sometimes opposing neural modulation effects observed [36]. In fact, the FUS we used in this study was previously shown to non-thermally stimulate compound muscle activation [7], [9]. In these sets of studies, we demonstrated the safety and efficacy of using high pressure FUS on the sciatic nerve using a combination of histological analysis and behavioral motor gait analysis. We did not see any direct damage to the nerve bundle or red blood cell extravasation in the surrounding muscle nor changes to the motor function of the mice. As accurate signaling to the brain is highly dependent upon fiber action potential frequency and patterns [37], additional FUS-induced excitability may cause interference or dispersion of action potentials, leading to decreased somatosensation, akin to theories using the gate theory of pain [38].

Nerve fiber hyperexcitability is a trademark of acute and chronic neuropathic pain. Given the evidence presented herein that FUS is likely capable of regulation of such fibers, we were motivated to investigate FUS modulation in the context of neuropathic pain. Our paired pulse experiment revealed interesting results that garner further study. We specifically conducted a paired-pulse experiment to study conditional pain sensitivity given that non-noxious electric stimulation can evoke pain depending on stimulation parameters [35]. We can clearly see this in the elevated levels of CBV and peak-to-peak values in the sham compared to the baseline measurements taken before FUS stimulation. Here, FUS did not enhance or decrease hemodynamic responses. However, SNI mice illustrates a different story. Without FUS intervention, pain responses increased dramatically from the start to the end of the experimental trial. In fact, SNI positive control mice had increases in the 2nd peak value indicating increased pain sensitivity to multiple electrical stimulations. But, in SNI mice that received FUS, this trend was reversed. Through FUS did not change initial pain response to the first stimulation, it reduced response to the second peak. Though not statistically significant, the trends indicated in Fig. 7 are in agreement with those in a previous study on FUS modulation of thermal pain in humans [25]. Here, we saw decreases in pain ratings when FUS was applied to the median nerve. Taken together, the findings in the current study were unexpected but without further experimentation, we can only hypothesize that FUS may be inhibiting the nerve's ability to conduct secondary pain responses. This will constitute the topic of additional future investigations.

These results begs the question, at what doses and how long does FUS neuromodulation last? Firstly, we observed lower levels of CBV changes lasting at least 14 minutes (total length of the experiment). Secondly, FUS lowered electrically-stimulated

CBV increases during and after sonication in SNI-FUS mice compared to FUS-sham, stabilizing and even decreasing peak-to-peak values after FUS, providing evidence that FUS may have longitudinal and potential compounding effects [24]. Preliminary functional connectivity analysis recorded over 30 minutes reveals distinct differences between wild-type and neuropathic pain mice with larger differences in the left hemisphere compared to the right (Fig. 6(d)–(g)). While our study probes functional characteristics of neuropathic pain, we only record functional changes at one time point. It would be both pertinent and interesting to see the functional progression of neuropathic pain from surgical intervention over several months. This way, we can control for the stages of neuropathic pain progression from acute to chronic more carefully, thus drawing more conclusive intuitions and providing further details about the offline effects of FUS.

## V. CONCLUSION

This study introduces a framework for studying FUS-based pain neuromodulation using high-resolution fUS imaging of the mouse brain. By imaging at 40 MHz using a 3/4th bandwidth sampling scheme and GPU-based beamformers, we were able to achieve an adequate frame rate for measuring hemodynamic changes in CBV in response to electrical, whisker, and FUS stimulation, as well as steady-state functional connectivity changes in neuropathic pain mice. Importantly, we saw that changes in FUS stimulation success rate were correlated with CBV changes. Additionally, by applying FUS stimulation to an acute model of neuropathic pain, we discovered that CBV in neuropathic pain mice rapidly increased in response to electrical stimulation at the nociceptive receptive fields. However, when stimulated with FUS, those responses were stabilized, signifying decreased pain sensation. These findings will help guide future study as we investigate FUS neuromodulation in human pain sensation and by elucidating a pathway in which FUS nerve stimulation produce analgesic effects, we anticipate that the insights developed in this study will help stimulate further research directions.

## ACKNOWLEDGMENT

The authors would like to thank Mr. Pablo Abreu for his gracious assistance, financially and administratively. We thank the Frank Morrel Endowed Memorial Scholarship and the Milton L. Shifman Endowed Scholarship for providing financial support to SAL to learn *in vivo* imaging techniques at the Neurobiology course at the Marine Biological Laboratory.

## REFERENCES

- [1] L. Colloca et al., "Neuropathic pain," *Nature Rev. Dis. Primers*, vol. 3, pp. 1–19, 2017.
- [2] V. Cotero et al., "Peripheral focused ultrasound neuromodulation (pFUS)," *J. Neurosci. Methods*, vol. 341, 2020, Art. no. 108721.
- [3] J. L. Foley, J. W. Little, and S. Vaezy, "Effects of high-intensity focused ultrasound on nerve conduction," *Muscle Nerve*, vol. 37, pp. 241–250, 2008.
- [4] V. Colucci et al., "Focused ultrasound effects on nerve action potential *in vitro*," *Ultrasound Med. Biol.*, vol. 35, pp. 1737–1747, 2009.

- [5] Y. F. Lee et al., "Nerve conduction block in diabetic rats using high-intensity focused ultrasound for analgesic applications," *Brit. J. Anaesth.*, vol. 114, pp. 840–846, 2015.
- [6] P. H. Tsui, S. H. Wang, and C. C. Huang, "In vitro effects of ultrasound with different energies on the conduction properties of neural tissue," *Ultrasonics*, vol. 43, pp. 560–565, 2005.
- [7] S. A. Lee et al., "Displacement imaging for focused ultrasound peripheral nerve neuromodulation," *IEEE Trans. Med. Imag.*, vol. 39, pp. 3391–3402, Nov. 2020.
- [8] C. J. Wright et al., "Unmyelinated peripheral nerves can be stimulated in vitro using pulsed ultrasound," *Ultrasound Med. Biol.*, vol. 43, pp. 2269–2283, 2017.
- [9] M. E. Downs et al., "Non-invasive peripheral nerve stimulation via focused ultrasound in vivo," *Phys. Med. Biol.*, vol. 63, 2018, Art. no. 035011.
- [10] P. D. Mourad et al., "Intense focused ultrasound preferentially stimulates transected nerves within residual limbs: Pilot study," *Pain Med.*, vol. 19, pp. 541–549, 2018.
- [11] P. P. Ye, J. R. Brown, and K. B. Pauly, "Frequency dependence of ultrasound neurostimulation in the mouse brain," *Ultrasound Med. Biol.*, vol. 42, pp. 1512–1530, 2016.
- [12] Y. Tufail et al., "Transcranial pulsed ultrasound stimulates intact brain circuits," *Neuron*, vol. 66, pp. 681–694, 2010.
- [13] K. Yoon et al., "Effects of sonication parameters on transcranial focused ultrasound brain stimulation in an ovine model," *PLoS One*, vol. 14, 2019, Art. no. e0224311.
- [14] R. F. Dallapiazza et al., "Noninvasive neuromodulation and thalamic mapping with low-intensity focused ultrasound," *J. Neurosurgery*, vol. 128, pp. 875–884, 2018.
- [15] D. Folloni et al., "Manipulation of subcortical and deep cortical activity in the primate brain using transcranial focused ultrasound stimulation," *Neuron*, vol. 101, pp. 1109–1116, 2019.
- [16] T. Deffieux et al., "Low-intensity focused ultrasound modulates monkey visuomotor behavior," *Curr. Biol.*, vol. 23, pp. 2430–2433, 2013.
- [17] J. Kubanek et al., "Remote, brain region-specific control of choice behavior with ultrasonic waves," *Sci. Adv.*, vol. 6, 2020, Art. no. eaaz4193.
- [18] W. Lee et al., "Transcranial focused ultrasound stimulation of human primary visual cortex," *Sci. Rep.*, vol. 6, 2016, Art. no. 34026.
- [19] E. Mace et al., "Functional ultrasound imaging of the brain: Theory and basic principles," *IEEE Trans. Ultrason., Ferroelect., Freq. Control*, vol. 60, no. 3, pp. 492–506, Mar. 2013.
- [20] C. Brunner et al., "Whole-brain functional ultrasound imaging in awake head-fixed mice," *Nature Protoc.*, vol. 16, pp. 3547–3571, 2021.
- [21] C. Demené et al., "Spatiotemporal clutter filtering of ultrafast ultrasound data highly increases doppler and fultrasound sensitivity," *IEEE Trans. Med. Imag.*, vol. 34, pp. 2271–2285, Nov. 2015.
- [22] A. A. Phillips et al., "Neurovascular coupling in humans: Physiology, methodological advances and clinical implications," *J. Cereb. Blood Flow Metab.*, vol. 36, no. 4, pp. 647–664, 2016.
- [23] H. Huang et al., "High-spatiotemporal-resolution ultrasound flow imaging to determine cerebrovascular hemodynamics in alzheimer's disease mice model," *Adv. Sci.*, vol. 10, no. 35, Dec. 2023, Art. no. 2302345.
- [24] T. H. H. Chao, J. H. Chen, and C. T. Yen, "Plasticity changes in forebrain activity and functional connectivity during neuropathic pain development in rats with sciatic spared nerve injury 11 medical and health sciences 1109 neurosciences," *Mol. Brain*, vol. 11, 2018, Art. no. 55.
- [25] S. A. Lee, H. A. S. Kamimura, and E. E. Konofagou, "Displacement imaging during focused ultrasound median nerve modulation: A preliminary study in human pain sensation mitigation," *IEEE Trans. Ultrason., Ferroelect., Freq. Control*, vol. 68, no. 3, pp. 526–537, Mar. 2021.
- [26] D. Garcia et al., "Stolt's f-k migration for plane wave ultrasound imaging," *IEEE Trans. Ultrason., Ferroelect., Freq. Control*, vol. 60, no. 9, pp. 1853–1867, Sep. 2013.
- [27] P. Kaczkowski, "Bandwidth sampling data acquisition with the vantage system for high frequency transducers verasonics reserves the right to change specifications without notice," *Verasonics White Paper*, pp. 1–5, May 2016.
- [28] A. Dizeux et al., "Functional ultrasound imaging of the brain reveals propagation of task-related brain activity in behaving primates," *Nature Commun.*, vol. 10, pp. 1–9, 2019.
- [29] C. C. Chang et al., "In vivo visualization of vasculature in adult zebrafish by using high-frequency ultrafast ultrasound imaging," *IEEE Trans. Biomed. Eng.*, vol. 66, no. 6, pp. 1742–1751, Jun. 2019.
- [30] H. C. Li et al., "In vivo visualization of brain vasculature in Alzheimer's disease mice by high-frequency micro-doppler imaging," *IEEE Trans. Biomed. Eng.*, vol. 66, no. 12, pp. 3393–3401, Dec. 2019.
- [31] C. S. Hubbard et al., "Behavioral, metabolic and functional brain changes in a rat model of chronic neuropathic pain: A longitudinal mri study," *NeuroImage*, vol. 107, pp. 333–344, 2015.
- [32] Y. Komaki et al., "Functional brain mapping using specific sensory-circuit stimulation and a theoretical graph network analysis in mice with neuropathic allodynia," *Sci. Rep.*, vol. 6, pp. 1–11, 2016.
- [33] B. U. Hoffman et al., "Focused ultrasound excites action potentials in mammalian peripheral neurons in part through the mechanically gated ion channel piezo2," *Proc. Nat. Acad. Sci.*, vol. 119, 2022, Art. no. e2115821119.
- [34] A. Urban et al., "Chronic assessment of cerebral hemodynamics during rat forepaw electrical stimulation using functional ultrasound imaging," *NeuroImage*, vol. 101, pp. 138–149, 2014.
- [35] L. Tøttrup et al., "Modulation of SI and ACC response to noxious and non-noxious electrical stimuli after the spared nerve injury model of neuropathic pain," *Eur. J. Pain*, vol. 25, pp. 612–623, 2021, doi: 10.1002/ejp.1697.
- [36] J. Kubanek et al., "Ultrasound modulates ion channel currents," *Sci. Rep.*, vol. 6, 2016, Art. no. 24170.
- [37] S. Panzeri et al., "Reading spike timing without a clock: Intrinsic decoding of spike trains," *Philos. Trans. Roy. Soc. B, Biol. Sci.*, vol. 369, 2014, Art. no. 20120467.
- [38] R. Melzack and P. D. Wall, "Pain mechanisms: A new theory," *Science*, vol. 150, pp. 971–979, 1965.